Tailoring Pore Structure of Ultralight Electrospun Sponges by Solid Templating

Fabian Deuber[a], Sara Mousavi[a,b], Marco Hoffer[c] and Christian Adlhart*[a]

Abstract: Freeze-casted nanofiber based sponges or aerogels exhibit a hierarchical porous structure. Pore formation is only partially understood. Therefore, we studied the underlying solid templating mechanism. We were able to tailor the secondary pore size between 9.5 and 123 µm while retaining the smaller primary pores known from electrospun nanofiber membranes. To understand the effect of microstructure on the sponges' bulk properties, mass flow through the pores and interaction with the sponges' internal surface were investigated. By solely altering the sponges' microstructure we indeed found tunability in permeability by a factor 7 and in filtration efficiency by a factor of 220. Hence, pore architecture of nanofiber based sponges is a key element for their performance. The selected pullulan/PVA polymer blends and aqueous electrospinning conditions are benign and allow the facile adaptation of these ultralight highly porous sponges for a large number of applications.

Nanofiber based materials obtained by electrospinning are intrinsically flat due to their layer by layer manufacturing process.[1] There are different routes to obtain 3D electrospun structures,[2] either by self-assembly,[3] cool drum spinning[4] or gas expansion. However they lack the possibility of adding scalable pores.[5] Recently, Ding and Greiner invented a new class of ultralight[6] truly 3D nanofiber based aerogel or sponge materials.[1a, 7] These materials reveal hierarchical pores: minor primary pores between tangled nanofibers, similar to those in electrospun membranes[8] and major cell-like secondary pores. We expect a tremendous effect on the sponges' macroscopic properties from these secondary pores, which is important for potential applications such as tissue scaffolds, catalyst supports, sound absorption or separation material.[1a, 7a] Fundamental bulk properties, which are governed by the porous microstructure are on the one hand air permeability as a mean to characterize mass flow through the sponge. Aerosol filtration on the other hand depends on diffusion within the pores and interaction with the internal surface of the sponge.

To tune size and shape of these secondary pores, we had to develop a fundamental understanding of their formation mechanism: basically, electrospun nanofibers are cut into short fibers,[9] dispersed in a non-solvent, and the liquid phase is subsequently exchanged with gas by freeze-drying.[1a, 7a, 10] This is similar to processing other nano rod/wire, fiber based,[11] or ceramic materials.[12]

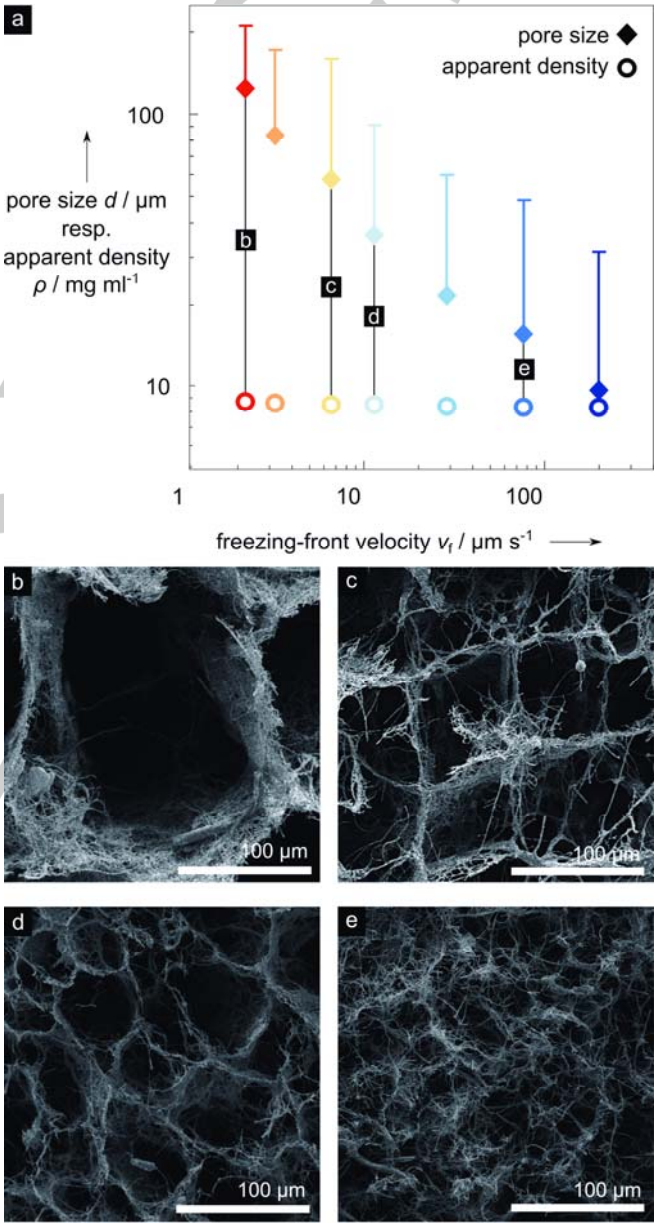

Figure 1. Effect of freezing conditions on sponge microstructure. (a) Slow freezing-front velocities, v_f, provide the largest pore diameters, d, while the sponges' apparent density remained constant within 8.7 ± 0.1 mg ml^{-1}. SEM images (b) to (e) show cross-sections of respective sponges at the center height of 7.5 mm obtained with different v_f. They exhibit clear open cellular hierarchical pore structures.

In this work, pullulan/PVA blend was selected as the nanofiber raw material for its compatibility with the thermal

[a] F. Deuber, Dr. C. Adlhart
Institute of Chemistry and Biotechnology, Zurich University of Applied Sciences ZHAW, 8820 Wädenswil, Switzerland
E-mail: christian.adlhart@zhaw.ch
[b] S. Mousavi
Department of Chemical Engineering
University of Sistan and Baluchestan
Blvd. Daneshgah, Zahedan, Iran
[c] M. Hofer
Incident Response and Individual Protection Branch
Federal Office for Civil Protection, Labor Spiez
Austrasse, 3700 Spiez, Switzerland

Supporting information for this article is given via a link at the end of the document.

cross-linking step,[13] its biodegradability and food compatibility.[14] Using free surface electrospinning we obtained uniform nanofibers with a diameter of 240 ± 55 nm. To synthesize the sponges, the nanofiber membranes were first homogenized in 1,4-dioxane to provide a suspension, which was subsequently frozen using a directional freezing approach. Sublimation yielded the desired raw bodies, which were eventually thermally cross-linked to ensure mechanical stability (the processing scheme and experimental details are given in the Supporting Information). The resulting ultralight (density between 4 and 19 mg ml^{-1}) and highly porous (porosity up to 99.8 %) fibrous network had directional pores along the thermal gradient, where the pores replicated the solvent's crystals. The resulting nanofiber based sponges showed the expected soft compressibility and bendability (Supporting Information, Tables S1 and S2).[1a, 7a, 10] By increasing the freezing-front velocity, v_f, from 2 to 200 µm s^{-1} (see Supporting Information, Figure S4) we can directly control the size of the secondary pores, decreasing from 123 to 9.5 µm, respectively, see Figure 1.

The shape of the secondary pores also depends on v_f: the large secondary pores reflect the structure of the monoclinic dioxane crystals[15] (Figure 1b and c), while the isotropic distribution of the short nanofibers in the starting suspension was preserved to a larger extent at faster v_f, Figure 1e . This is understood by the accepted freezing mechanism for nanoparticle slurries,[12] where the dispersed nanoparticles are rejected by the moving solidification front and thus are concentrated between the growing crystals.[12c, 12d, 16] It is the velocity of the growing crystals that determines whether a particle, or in our case, the fiber inside the slurry will be rejected and pushed away, or if they will be trapped and embedded into the growing crystal.[17] The small pores in Figure 1e therefore indicate that the solidification front was faster than the mobility of the fibers. The slower the freezing-front, the more redistribution and rejection of the short fibers is possible, thus resulting in larger pores, Figure 1b and c.[12d, 16] Close to the contact area with the heat sink, crystal propagation is dominated by nucleation, which leads to different freezing zones. Such details have been elaborated for ceramic based materials.[18]

The secondary pore size does also depend on the solid loading of the nanofiber slurry. When keeping v_f constant at 6.24 µm s^{-1} but changing the solid loading between 0.260 %, 0.564 %, and 1.174 % (*V*/*V* – see Supporting Information), the pore size decreased from 71.2 µm and 56.7 µm down to 28.8 µm (Figure S9). This is understood based on the viscosity of the slurry, which is increased by higher solid loading. Thereby mobility of the fibers is decreased and embedding into the growing crystals is favored – thus giving smaller pores. Quantitative models for this observation have been derived for particle containing slurries: the critical freezing front velocity, v_{crit}, at which particle entrapment and thus formation of smaller pores takes place, depends inversely proportional on the viscosity of the slurry.[17b, 19]

The significant difference in the sponges' microstructure with pores ranging from 9.5 to 123 µm should also be reflected in the bulk properties of the material. Therefore, we investigated the gas mass flow as well as the aerosol filtration efficiency, since these properties are fundamental in understanding how the pore size of the material governs its macroscopic characteristics.

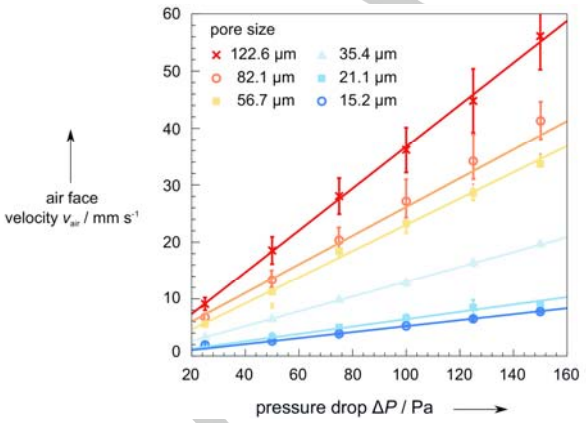

Figure 2. Effect of pressure drop, Δ*P*, on air face velocity, v_{air}, for nanofiber-based sponges with similar apparent density of 8.7 ± 0.1 mg ml^{-1}, but different pore size. Sample thickness was 15 mm. K_{air}, is 1.45 x 10^{-11}, 1.79 x 10^{-11}, 3.61 x 10^{-11}, 6.60 x 10^{-11}, 7.10 x 10^{-11}, and 1.02 x 10^{-10} m^2.

Figure 2 shows the effect of variable pressure drop, Δ*P*, on the air face velocity, v_{air} for nanofiber based sponges with identical apparent density but different pore size. Using the Hagen-Poiseuille equation[20] for compressible fluids through porous material, permeability, K_{air} was calculated to be between 1.45 x 10^{-11} m^2 for the smallest and 1.02 x 10^{-10} m^2 for the largest pores (see Supporting Information, Table S2). These values are exceeding those of melt spun, 8.30 x 10^{-12} m^2, electrospun, 6.96 x 10^{-14} m^2, or ice templated ceramics (10^{-14} m^2 to 10^{-11} m^2)[21] highlighting the potential of nanofiber based sponges, especially, since the permeability in electrospun nanofiber membranes is mainly controlled by thickness[8a] whereas the freezing process in sponge processing adds a second variable to tailor permeability by at least a factor of 7.

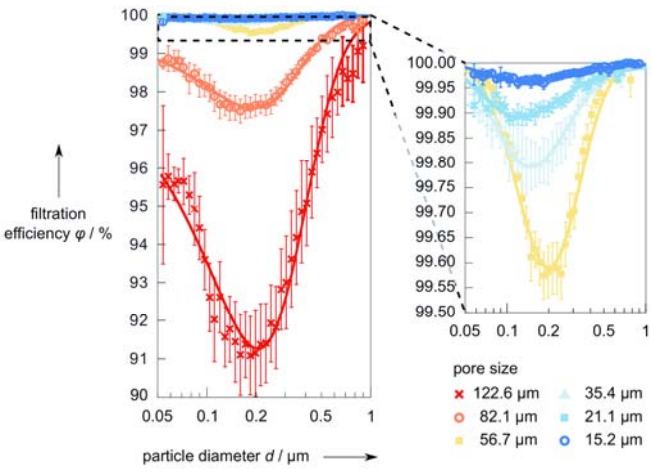

Figure 3. Particle filtration efficiency, φ, of nanofiber-based sponges with tailored pore size. Face velocity v_{air} of 1.5 cm s^{-1}. Sponges with an apparent

density of 8.7 ± 0.1 mg ml^{-1} were used. Data are fitted according to the semi empirical efficiency model by Lee and Liu.[22] Most penetrating particle size, MPPS, and φ@MPPS are 202 nm (91.22 %), 159 nm (97.46 %), 200 nm (99.59 %), 148 nm (99.79 %), 134 nm (99.87 %), 143 nm (99.96 %).

Diffusion within the pores and interaction with the nanofiber based internal surface of the sponges are fundamental processes in aerosol filtration. Moreover, aerosol filtration and in fact every process requiring mass exchange between a stationary and a mobile phase are a compromise between high permeability and high efficiency.

Figure 3 shows the effect of filtration efficiency of nanofiber based sponges solely depending on the dimension of the secondary pores, while thickness and apparent density of the material were kept constant. Filtration efficiency increased tremendously from 91.22 % for the largest pores to 99.96 % for the smallest pores, meaning a decrease of penetrated aerosol by a factor of 220. However, the most penetrating particle size, MPPS, remained constant within a factor of 1.54 (from 134 to 202 nm). Theoretical models predict a modest dependence of the MPPS on the fiber diameter (and thus pore size),[23] and similar MPPS values between 170 and 225 nm are reported for melt blown filters with fiber diameters from 0.5 to 2 µm.[24] Typical MPPS values for nanofiber based membranes are < 80 nm.

To put nanofiber sponge filters into further context with other (nano)fiber-based filtration materials, a trade-off parameter called quality factor (QF) can be calculated:[25] QF = - ln(1-φ)/ΔP, where φ is the filtration efficiency and ΔP the pressure drop. Our sponge-like filters had a QF between 0.027 and 0.087 Pa^{-1} (see Supporting Information, Table S2). We measured and calculated QF values for commercially available melt blown membranes (QF = 0.032 Pa^{-1}), nanofiber membranes (QF = 0.019 Pa^{-1}), and the classical Petrayanov filter (QF = 0.048 Pa^{-1}). Other electrospun[26] and melt spun[26d, 27] nanofiber filters are in a similar range regarding QF, however when combining electrospun nanofibers with 'nanonetting' a QF of 0.25 Pa^{-1} can be achieved.[28] Yet, nanofiber based sponges may prove a drastically higher dust holding captivity, for they act as deep bed filtration materials.[10c]

Processing nanofibers into sponges is almost as straightforward as electrospinning.[1b-d] Following the pioneering work of Ding[1a] and Greiner[7a], we have shown, how carbohydrate based electrospun nanofibers can be processed into ultralight sponges with a hierarchical and tunable pore structure. Primary pores are caused by tangled fibers whereas the larger secondary ones are controlled by the velocity of the solidification front of the freezing liquid. These secondary pores were tailored between 123 µm and 9.5 µm, which is similar to the pore size observed for ceramic based materials (2 µm to 200 µm, depending on the system).[12b-e, 16, 29] A tremendous effect of the secondary pore structure was seen in air permeability and in filtration efficiency, which varied between a factor of 7 and 220, respectively.

Understanding the solid templated generation of the nanofiber based sponges' microstructure allows to efficiently designing their macroscopic characteristics. We believe that the microstructure of nanofiber based sponges is a key element for their performance in many anticipated applications, whether as scaffold for tissue engineering, as catalyst support, or their use in filtration. We also envision materials with anisotropic properties caused by directed growth of the solid template crystals.

Experimental Section

Experimental details regarding electrospinning process, 3D nanofiber sponge processing, and further physical chemical characterization including FTIR, *E*-Modulus, plastic deformation, porosity, pressure drop at air face velocity, v_{air} = 1.5 cm s^{-1}, and air face velocity at 250 Pa according to ASTM D3574-11, as well as details regarding the investigated commercial filtration materials are given in the Supporting Information.

Acknowledgements

This work was supported by Forschungsfond Aargau, IVF-Hartmann AG (Thesis of F. D.), and COST ACTION MP1206 (travelling grants).

Keywords: aerogel • crystal growth • electrospinning • freeze-casting • nanostructures

[1] a) Y. Si, J. Yu, X. Tang, J. Ge, B. Ding, *Nat. Commun.* **2014**, *5*, 5802; b) J. H. Wendorff, S. Agarwal, A. Greiner, *Electrospinning: Materials, Processing, and Applications*, Wiley-VCH, Weinheim, **2012**; c) A. Greiner, J. H. Wendorff, *Angew. Chem. Int. Ed* **2007**, *46*, 5670; d) W. E. Teo, S. Ramakrishna, *Nanotechnology* **2006**, *17*, R89; e) R. Buttiker, J. Ebert, C. Hinderling, C. Adlhart, *Chimia* **2011**, *65*, 182.

[2] B. Sun, X.-J. Jiang, S. Zhang, J.-C. Zhang, Y.-F. Li, Q.-Z. You, Y.-Z. Long, *J. Mater. Chem. B* **2015**, *3*, 5389.

[3] a) B. Sun, Y.-Z. Long, F. Yu, M.-M. Li, H.-D. Zhang, W.-J. Li, T.-X. Xu, *Nanoscale* **2012**, *4*, 2134; b) X. Guo, Y. Yao, T. Zhou, R. Xiang, M. Chen, *J. Appl. Polym. Sci.* **2015**, *133*, 43003; c) G. Chang, X. Zhu, A. Li, W. Kan, R. Warren, R. Zhao, X. Wang, G. Xue, J. Shen, L. Lin, *Mater. Des.* **2016**, *97*, 126.

[4] M. Simonet, O. D. Schneider, P. Neuenschwander, W. J. Stark, *Polym. Eng. Sci.* **2007**, *47*, 2020.

[5] J. Rnjak-Kovacina, A. S. Weiss, *Tissue Eng., Part B* **2011**, *17*, 365.

[6] S. Chabi, V. G. Rocha, E. García-Tuñón, C. Ferraro, E. Saiz, Y. Xia, Y. Zhu, *ACS Nano* **2016**, *10*, 1871.

[7] a) G. Duan, S. Jiang, V. Jérôme, J. H. Wendorff, A. Fathi, J. Uhm, V. Altstädt, M. Herling, J. Breu, R. Freitag, S. Agarwal, A. Greiner, *Adv. Funct. Mater.* **2015**, *25*, 2850; b) Y. Si, X. Wang, C. Yan, L. Yang, J. Yu, B. Ding, *Adv. Mater.* **2016**, DOI 10.1002/adma.201603143.

[8] a) P. Gibson, H. Schreuder-Gibson, D. Rivin, *Colloids Surf., A* **2001**, *187-188*, 469; b) D. Li, M. W. Frey, Y. L. Joo, *J. Membr. Sci.* **2006**, *286*, 104.

[9] a) J. s. Kim, D. H. Reneker, *Polym. Compos.* **1999**, *20*, 124; b) M. Langner, A. Greiner, *Macromol. Rapid Commun.* **2016**, *37*, 351; c) S. Jiang, G. Duan, J. Schöbel, S. Agarwal, A. Greiner, *Compos. Sci. Technol.* **2013**, *88*, 57.

[10] a) G. Duan, S. Jiang, T. Moss, S. Agarwal, A. Greiner, *Polym. Chem.* **2016**, *7*, 2759; b) T. Xu, J. M. Miszuk, Y. Zhao, H. Sun, H. Fong, *Adv. Healthcare Mater.* **2015**, *4*, 2238; c) Y. Si, Q. Fu, X. Wang, J. Zhu, J. Yu, G. Sun, B. Ding, *ACS Nano* **2015**, *9*, 3791; d) W. Chen, J. Ma, L. Zhu, Y. Morsi, H. El-Hamshary, S. S. Al-Deyab, X. Mo, *Colloids Surf., B* **2016**, *142*, 165.

[11] a) L. Qiu, J. Z. Liu, S. L. Y. Chang, Y. Wu, D. Li, *Nat. Commun.* **2012**, *3*, 1241; b) X. Gui, J. Wei, K. Wang, A. Cao, H. Zhu, Y. Jia, Q. Shu, D. Wu, *Adv. Mater.* **2010**, *22*, 617; c) Z.-Y. Wu, C. Li, H.-W. Liang, J.-F. Chen, S.-H. Yu, *Angew. Chem. Int. Ed* **2013**, *52*, 2925; d) P. Munier, K. Gordeyeva, L. Bergström, A. B. Fall, *Biomacromolecules* **2016**, *17*, 1875.

[12] a) Y. Zhou, S. Fu, Y. Pu, S. Pan, A. J. Ragauskas, *Carbohydr. Polym.* **2014**, *112*, 277; b) W. L. Li, K. Lu, J. Y. Walz, *Int. Mater. Rev.* **2013**, *57*, 37; c) S. Deville, *Adv. Eng. Mater.* **2008**, *10*, 155; d) S. Deville, E. Saiz, R. K. Nalla, A. P. Tomsia, *Science* **2006**, *311*, 515; e) N. O. Shanti, K. Araki, J. W. Halloran, *J. Am. Ceram. Soc.* **2006**, *89*, 2444; f) K. Araki, J. W.

Halloran, *J. Am. Ceram. Soc.* **2005**, *88*, 1108; g) T. Fukasawa, Z. Y. Deng, M. Ando, T. Ohji, Y. Goto, *J. Mater. Sci.* **2001**, *36*, 2523.
[13] S. Islam, S. Rahaman, J. H. Yeum, *Carbohydr. Polym.* **2015**, *115*, 69.
[14] a) T. D. Leathers, *Appl. Microbiol. Biotechnol.* **2003**, *62*, 468; b) Y. F. Qian, L. J. Zheng, R. Y. Song, B. Du, *Adv. Mater. Res.* **2013**, *821-822*, 1321.
[15] J. Buschmann, E. Müller, P. Luger, *Acta Crystallogr. Sect. C: Cryst. Struct. Commun.* **1986**, *42*, 873.
[16] U. G. K. Wegst, M. Schecter, A. E. Donius, P. M. Hunger, *Philos. Trans. R. Soc. London, Ser. A* **2010**, *368*, 2099.
[17] a) R. Asthana, S. N. Tewari, *J. Mater. Sci.* **1993**, *28*, 5414; b) G. Lipp, C. Körber, *J. Cryst. Growth* **1993**, *130*, 475.
[18] a) S. Deville, E. Saiz, A. P. Tomsia, *Biomaterials* **2006**, *27*, 5480; b) S. Deville, E. Maire, A. Lasalle, A. Bogner, C. Gauthier, J. Leloup, C. Guizard, *J. Am. Ceram. Soc.* **2009**, *92*, 2489; c) Z. Hou, F. Ye, L. Liu, *J. Eur. Ceram. Soc.* **2015**, *35*, 4115.
[19] H. F. Zhang, I. Hussain, M. Brust, M. F. Butler, S. P. Rannard, A. I. Cooper, *Nat Mater* **2005**, *4*, 787.
[20] M. A. Sanjuan, R. Muñoz-Martialay, *Building and Environment* **1997**, *32*, 51.
[21] J. Seuba, S. Deville, C. Guizard, *Sci. Technol. Adv. Mat.* **2016**, accepted manuscript.
[22] a) K. W. Lee, B. Y. H. Liu, *Aerosol Sci. Technol.* **1982**, *1*, 147; b) D. Boulaud, A. Renoux, in *Advances in Aerosol Gas Filtration* (Ed.: K. R. Spurny), CRC Press **1998**, pp. 53.
[23] A. Podgorski, A. Balazy, L. Gradon, *Chem. Eng. Sci.* **2006**, *61*, 6804.
[24] M. Lalagiri, G. Bhat, V. Singh, S. Parameswaran, R. J. Kendall, S. Ramkumar, *Industrial & Engineering Chemistry Research* **2013**, *52*, 16513.
[25] I. B. Stechkina, N. A. Fuchs, *Ann. Occup. Hyg.* **1966**, *9*, 59.
[26] a) Y. Yang, S. Zhang, X. Zhao, J. Yu, B. Ding, *Sep. Purif. Technol.* **2015**, *152*, 14; b) C.-H. Hung, W. W.-F. Leung, *Sep. Purif. Technol.* **2011**, *79*, 34; c) W. Sambaer, M. Zatloukal, D. Kimmer, *Chem. Eng. Sci.* **2011**, *66*, 613; d) R. Gopal, S. Kaur, Z. Ma, C. Chan, S. Ramarishna, T. Matsuura, *J. Membr. Sci.* **2006**, *281*, 581.
[27] M. A. Hassan, B. Y. Yeom, A. Wilkie, B. Pourdeyhimi, S. A. Khan, *J. Membr. Sci.* **2013**, *427*, 336.
[28] a) N. Wang, Y. Yang, S. S. Al-Deyab, M. El-Newehy, J. Yu, B. Ding, *J. Mater. Chem. A* **2015**, *3*, 23946; b) B. Liu, S. Zhang, X. Wang, J. Yu, B. Ding, *J. Colloid Interface Sci.* **2015**, *457*, 203; c) Y.-Y. Kuo, F. C. Bruno, J. Wang, *Aerosol Sci. Technol.* **2014**, *48*, 1332.
[29] a) M. M. Porter, J. Mckittrick, M. A. Meyers, *JOM* **2013**, *65*, 720; b) S. Deville, *Materials* **2010**, *3*, 1913; c) S. Deville, E. Saiz, A. P. Tomsia, *Acta Mater.* **2007**, *55*, 1965.

WILEY-VCH

Entry for the Table of Contents

Layout 1:

COMMUNICATION

Growing nanostructures: Assembling short electrospun nanofibers in a controlled way yields highly porous 3D materials. Their bulk properties in terms of mass flow, diffusion, and interaction with internal surface are meticulously adjusted through the microstructure of the nanofiber assembly which is steered by the freeze-casting conditions. This insight is central in tailoring future function and properties of 3D electrospun sponges.

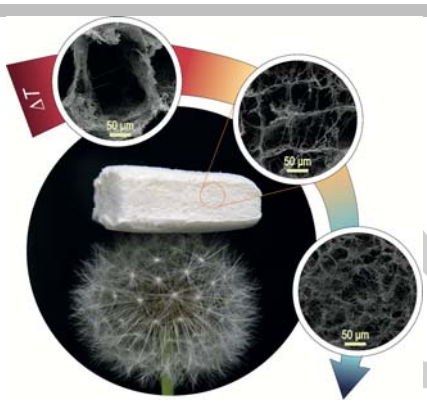

*Fabian Deuber, Sara Mousavi, Marco Hoffer, Christian Adlhart**

Page No. – Page No.

Tailoring pore structure of ultralight electrospun sponges by solid templating

WILEY-VCH